Catalysis Today 175 (2011) 65–71

Contents lists available at ScienceDirect

Catalysis Today

journal homepage: www.elsevier.com/locate/cattod

CeO_2–CoO_x mixed oxides: Structural characteristics and dynamic storage/release capacity

Jianqiang Wang[a,b], Meiqing Shen[a,c,*], Jun Wang[a], Jidong Gao[b], Jie Ma[b], Shuangxi Liu[b]

[a] Key Laboratory for Green Chemical Technology of State Education Ministry, School of Chemical Engineering & Technology, Tianjin University, Tianjin 300072, PR China
[b] China Automotive Technology & Research Center, Tianjin 300162, PR China
[c] State Key Laboratory of Engines, Tianjin University, Tianjin 300072, PR China

ARTICLE INFO

Article history:
Received 13 October 2010
Received in revised form 15 February 2011
Accepted 1 March 2011
Available online 2 April 2011

Keywords:
CoO_x–CeO_2
Solubility limit
Dynamic oxygen storage/release capacity
Compensation effect

ABSTRACT

CoO_x–CeO_2 mixed oxides with increasing Co/(Ce + Co) atomic ratio (1–20 mol%) are prepared by sol–gel method and characterized by means of by X-ray powder diffraction (XRD), Brunauer–Emmett–Teller (BET) and Hydrogen temperature-programmed reduction (H_2-TPR) techniques. The dynamic oxygen storage capacity (DOSC) is investigated by mass spectrometry with CO/O_2 transient pulses. The powder XRD data following Rietveld refinement reveal that the solubility limit of cobalt oxides in the CeO_2 was 5 mol% based on Co/(Ce + Co). The lattice parameters have been observed to experience a decrease followed by an increase due to the influence of the maximum solubility limit of cobalt oxides in the CeO_2. TPR analysis reveals that Co introduction into ceria strongly modifies the textual and structural properties, which influenced the oxygen handling properties. DOSC results reveal that Ce-based materials containing Co oxides with multiple valences contribute to the majority of DOSC. The kinetic analysis indicates that the calculated apparent kinetic parameters obey the compensation effect.

1. Introduction

Oxygen storage materials (OSMs) have become important after the introduction of catalytic treatment of automotive exhaust in early 1970s. Three-way catalysts that can eliminate CO, HCs (hydrocarbons), and NO_x simultaneously have been used to control exhaust emissions. The oxygen storage capacity (OSC) associated with a fast Ce(IV)/Ce(III) redox process, is one of the key properties of OSMs [1]. Various studies have shown that the reducibility and catalytic activity of CeO_2 can be considerably enhanced by doping with small amounts of transition metals [1,2]. This is because the high cost of noble metal catalysts such as Pt and Pd constitutes an economic limit for their industrial applications, despite their catalytic efficiency toward important reactions, such as low temperature CO oxidation. These considerations are at the basis of a considerable scientific and technological effort for introducing reactive transition metal ions into the ceria lattice, with the goal of identifying their role into the catalytic processes and engineering the defect chemistry accordingly.

Recently more and more research is focusing on new catalysts containing cheaper transition metals with relatively high activity and fairly good stability. Co_3O_4 shows the highest catalytic activity for the combustion of carbon monoxide and of organic compounds and it may be included in formulation of catalyst for treatment of waste gases [3]. Moreover, cobalt oxides are an attractive choice in the hydrocracking process of crude fuels, in several oxidation reactions, as well as in ammonia oxidation [4,5]. By utilizing the oxygen buffering effect, CoO_x–CeO_2 catalysts have attracted great attention for low-temperature CO oxidation, methanol oxidation, CH_4 combustion, diesel soot oxidation, N_2O decomposition and Fischer–Tropsch synthesis [6–14]. During these reactions, a catalytic synergistic effect between cobalt and cerium oxides is observed, especially for the oxidation reaction. Furthermore, the interactions between the ceria and Co could also change the electronic properties of Co, which results in the enhancement of its catalytic reactivity. However, according to Noronha et al. [15], precious metal particles were covered by aggregated transition metal species after redox ageing, and this is going to decrease the catalytic activity severely. In order to make good utilization of transition metal but not to poison the precious metals, it is very necessary fix after the dopants in the lattice during the ageing. The improvement of the catalytic activity and resistance to high temperature of these alternative systems would be desirable in order to use them as co-catalysts and, therefore, reduce the amount of expensive precious metals in conventional catalytic devices. Further, it is desirable to determine the effect of dopants on the lattice parameters and their solubility limits in the cubic fluorite structure phase. Tailoring the physical properties and adding new functionality to the existing

* Corresponding author at: Key Laboratory for Green Chemical Technology of State Education Ministry, School of Chemical Engineering & Technology, Tianjin University, Tianjin 300072, PR China. Tel.: +86 22 27892301; fax: +86 22 27892301.
E-mail address: mqshen@tju.edu.cn (M. Shen).

0920-5861/$ – see front matter © 2011 Elsevier B.V. All rights reserved.
doi:10.1016/j.cattod.2011.03.004

materials by engineering the structure, composition, and particle and/or grain size are among the new approaches in advancing the current applications of materials.

As a matter of fact, despite the promising behavior of cobalt oxides and ceria, only few papers concern the solid solution containing cobalt and cerium; moreover, they are only focused on the catalytic activity of mixed oxides, while solid solution could be an interesting choice. The present contribution focuses on the $Co_xCe_{1-x}O_y$ solubility limits by XRD Rietveld refinement analysis. The dynamic oxygen storage capacity (DOSC) of $Co_xCe_{1-x}O_y$ samples was investigated. The relationship between solid solution and its activity for DOSC and the structure was proposed.

2. Experimental

2.1. Sample preparation

Co doping ceria mixed oxides ($Co_xCe_{1-x}O_y$, x = 0.01, 0.03, 0.05, 0.07, 0.1, 0.15, 0.2) were synthesized by citric acid sol–gel method. The nitrates of Ce and Co were used as starting materials. Citric acid was added as complex agent, and glycol was used as additive. After continuous stirring for 2 h, the mixed solution was treated at the temperature of 353 K overnight to form the sponge yellow gel. Then, the gel was dried at 373 K for 3 h and milled before calcination. The dried gel was calcined at 573 K for 30 min and then at 773 K for 5 h. In this way, the fresh sample was obtained. The samples further were calcined at 973 K, 1073 K and 1173 K in air for 3 h and referred to as $Co_{0.05}Ce_{0.95}O_x$(1173 K), $Co_{0.1}Ce_{0.9}O_x$(973 K), $Co_{0.1}Ce_{0.9}O_x$(1073 K) and $Co_{0.1}Ce_{0.9}O_x$(1173 K), respectively. The CeO_2 prepared with the same method were reference samples.

2.2. Characterization

The structure of the mixed oxides was identified by X-ray diffraction (XRD) on an X'Pert Pro diffractometer using Fe-filtered Co Kα radiation and a power of 45 kV × 30 mA. The intensity data were collected at 298 K over a 2θ range of 20–90° with a 0.03° step size.

The X-ray diffraction analyses were carried out at room temperature on a Rigaku D/max 2500 v/pc diffractometer with Cu Kα radiation a power of 40 kV × 20 mA. The intensities of the XRD patterns were obtained in the 2θ range between 20° and 90° with a step of 0.02° and a measuring time of 2.0 s each point. The MAUD (material analysis using diffraction) software was applied to refine the crystalline structures of the solids with the Rietveld method.

H_2-TPR experiments were performed using a Micromeritics AutoChem 2910. The catalyst was first purged under N_2 (30 mL/min) at 200 °C for 1 h and then cooled to room temperature. The sample was then exposed to a flow of 5% H_2/Ar (30 mL/min) while the temperature was ramped from room temperature to 900 °C at a rate of 10 °C/min.

2.3. Dynamic oxygen storage capacity

Two types of OSC measurements were conducted, including dynamic CO–He pulses and transient CO–O_2 pulses [16]. Concentrations of CO, O_2, CO_2, Ar, and He in the outlet gas were monitored online by Hiden HPR20 quadrupole mass spectrometer. 25 mg sample diluted with 40 mg quartz sand was placed in the heat transfer reactor (10 mm diameter) at a height of 1.5 mm, with additional 4 mm redistributing layers of quartz wool on the two sides of catalysts bed. Flow rate of every pulse is 300 mL/min. Dead volume of the system was 3.5 mL. Errors induced by residence time and possible CO + O_2 turbulent mixing involved catalytic combustion can be limited to 2% during OSC quantifications. Before both of the testing

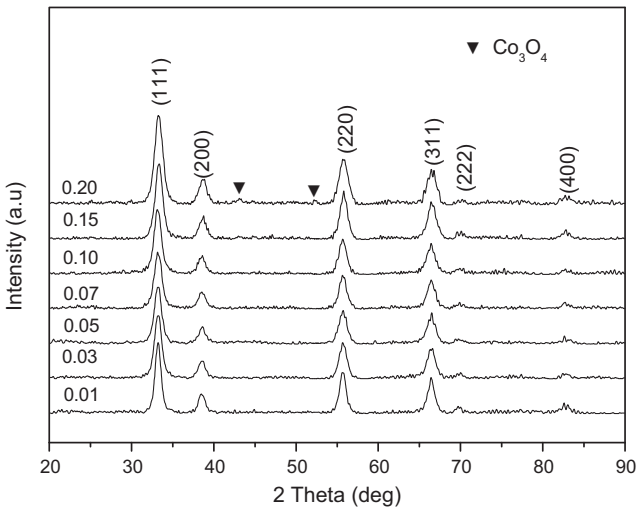

Fig. 1. XRD pattern of $Co_xCe_{1-x}O_y$ (x = 0.01, 0.03, 0.05, 0.07, 0.1, 0.15, 0.2).

modes, samples were pre-oxidized under 2% O_2/1% Ar/He atmosphere, and then purged under He until no $^{32}O_2$ signal detected. The two experimental modes are described as the follows: (1) Transient oxygen release measurements at 773 K were conducted under consecutive CO (5 s)–He (40 s) conditions. 4% CO/1% Ar/He and He were alternately pulsed for 10 times in sequence. (2) Dynamic CO–O_2 pulses (DOSC) measurements were operated from 473 to 773 K with the interval of 100 K. At each testing temperature, 4% CO/1% Ar/He and 2% O_2/1% Ar/He were pulsed alternately in sequence at the frequency of 0.1 Hz. The simulated plug flows repeated for more than 5 cycles to guarantee the reproducibility of collected response curves.

3. Results and discussion

3.1. Characterization

3.1.1. XRD analysis

Fig. 1 illustrates the powder XRD patterns of the as prepared samples of $Co_xCe_{1-x}O_y$ at different dopant contents. The diffraction peaks were indexed to (1 1 1), (2 0 0), (2 2 0), (3 1 1), (2 2 2) and (4 0 0) planes, matching well those of the face-centered cubic fluorite structure of CeO_2 (JCPDS No. 43-1002). It can be seen that no CoO_x phases (CoO or Co_3O_4) can be identified for Co/(Ce + Co) ratios lower than 0.15. This demonstrates that cobalt oxide exists as highly dispersed or amorphous surface species or the cobalt amount is low. However, apparent CoO_x peaks appear when x > 0.2. From Fig. 1, it is seen that all diffraction peaks were broadened, which indicated the fine nature of the small particles, in agreement with previous result [12].

The lattice parameters of the as-prepared $Co_xCe_{1-x}O_y$ samples were calculated by Rietveld refinement analysis. The Rietveld's method has given a reasonable fit of the diffraction profiles (R_{wp} < 15%). As shown in Fig. 2, it indicated that the XRD pattern could be indexed satisfactorily to the fluorite structure with a space group $Fm3m$. The values of the lattice parameters and lattice strain for all the samples are listed in Table 1. The relationship between the lattice parameter and the content of dopant cobalt is shown in Fig. 3. With increasing Co content, the lattice parameter for the fluorite solid solutions decreases linearly up to 5.4018(10) Å for x < 0.05. It is reasonable that cobalt ions have been incorporated into the CeO_2 lattice to form solid solutions by considering the radius of Co ions ($r_{Co}^{2+} = 0.075$ nm; $r_{Co}^{3+} = 0.061$ nm) is smaller than that of Ce^{4+} ions (0.101 nm). In the typical cubic fluorite lattice of CeO_2, Ce(IV)

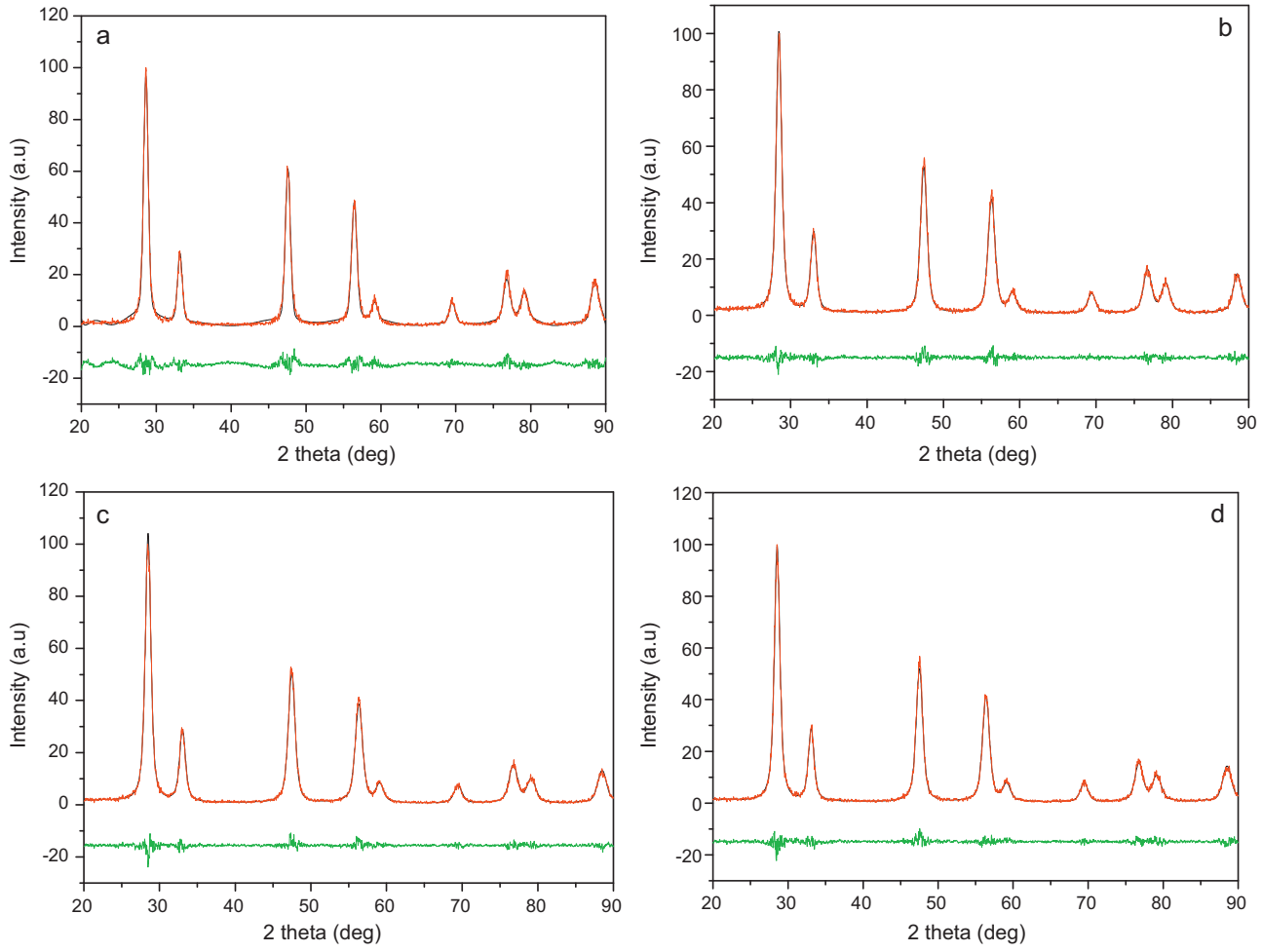

Fig. 2. Rietveld refinement plots of the $Co_xCe_{1-x}O_y$: (a) $Co_{0.01}Ce_{0.99}O_y$; (b) $Co_{0.03}Ce_{0.97}O_y$; (c) $Co_{0.05}Ce_{0.95}O_y$; (d) $Co_{0.07}Ce_{0.93}O_y$.

cations occupy one-half cube interstitial sites and are coordinated by eight oxygen ions. When Co ions (II or III) are incorporated into the Ce(IV) sites, oxygen nonstoichiometry is essential because of charge compensation, i.e, with increasing content of the dopant, the coordination of the Ce(IV) is lower than 8-fold, and the concentration of the oxygen vacancies ($Vo^{\bullet\bullet}$) or/and complex defect associations will increase. Additionally, the effective ionic radius of Co is smaller than that of Ce(IV). These factors account for the linear decrease of the lattice parameter with dopant content. It is noteworthy that the lattice parameter for $Co_{0.07}Ce_{0.93}O_y$ is significantly increased, suggesting that the cobalt ions segregate gradually from $Co_xCe_{1-x}O_y$ solid solutions with further increase of Co content. So we can conclude that the solution limit of CoOx in ceria is 5%. Further, we calculate the theoretic lattice parameters of different $Co_xCe_{1-x}O_y$ samples according to Vegard's law. The experimental lattice parameters are slightly larger than the theoretic values. This implies the existence of Ce^{3+}(1.14 Å). According to Kim [17], the solubility limits of one element in the fluorite ceria oxides were related to the ionic size difference between the dopant cation and host cation. For a substitutional solid solution, the extent of solid solubility of various elements in a given host crystal lattice can be expressed as a function of the radius difference between the solute and host element and the valency of the solute. When a cation whose radius and valency are different from those of the host cation is introduced into the fluorite lattice, it creates a strain in the lattice unless the influences of the two factors cancel each other out. The elastic energy in the strained lattice governs the extent of the solid solution in such a way that the smaller the energy required to introduce a dopant cation, the wider the extent of solid solubility of the dopant. Glushkova et al. [18] have taken account of the influence of both the radius difference and anion vacancy formation on the change of the lattice parameter. The contraction of the lattice due to the creation of oxygen-ion vacancies is incorporated through the consideration of the effective oxygen-ion radius, which becomes smaller as the dopant concentration increases.

Fig. 4 shows the effects of calcination temperature on the XRD patterns of $Co_{0.05}Ce_{0.95}O_y$ and $Co_{0.1}Ce_{0.9}O_y$ samples. The diffraction peaks of the samples were getting sharpened after calcination, because of their larger crystal sizes. The calcined $Co_{0.05}Ce_{0.95}O_y$ still remained the single fluorite structure, whereas the calcined

Table 1
Results of texture characterizations for $Co_xCe_{1-x}O_y$ samples.

Sample	BET (m^2/g)	Lattice parameters (Å)	Lattice strain	R_{wp} (%)	Theoretic lattice parameters (Å)
$Co_{0.01}Ce_{0.99}O_y$	37.1	5.4196 (11)	0.108 (27)	7.74	5.4036
$Co_{0.03}Ce_{0.97}O_y$	41.5	5.4049 (11)	0.202 (21)	10.95	5.3847
$Co_{0.05}Ce_{0.95}O_y$	39.4	5.4018 (10)	0.259 (16)	9.97	5.3674
$Co_{0.07}Ce_{0.93}O_y$	33.3	5.4095 (11)	0.244 (16)	11.21	5.3456

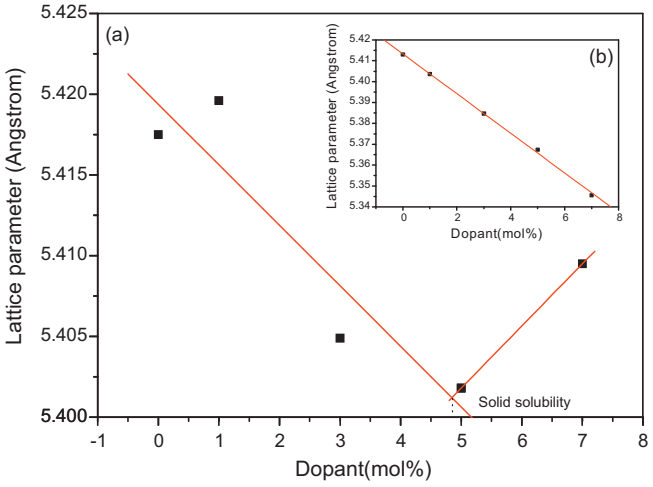

Fig. 3. Dependence of the lattice parameter with [Co]/([Co]+[Ce]) (a) the lattice parameters based on XRD Rietveld refinement; (b) the theoretic lattice parameters based on Vegard's law.

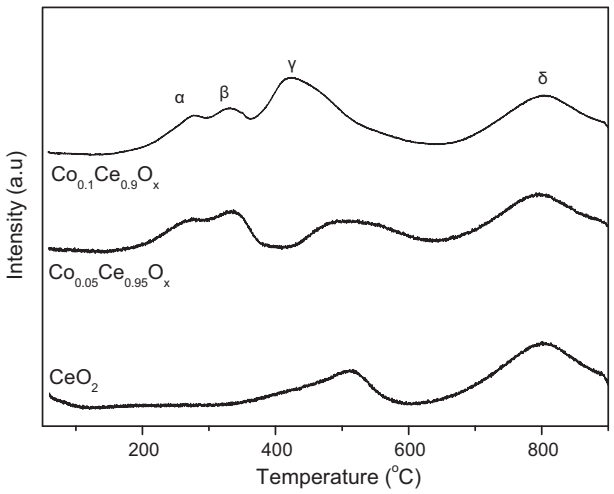

Fig. 5. H_2-TPR profiles of (1) CeO_2 (2) $Co_{0.05}Ce_{0.95}O_x$ (3) $Co_{0.1}Ce_{0.9}O_x$ samples.

$Co_{0.1}Ce_{0.9}O_y$ showed visible CoO_x phases. The redundant cobalt ions segregate gradually from $Co_xCe_{1-x}O_y$ solid solutions with further increase of Co content. It suggested that the solid solution behave superior thermal stability.

3.1.2. H_2-TPR

H_2-TPR profiles of Co doped samples ($Co_{0.05}Ce_{0.95}O_y$ and $Co_{0.1}Ce_{0.9}O_y$) and reference samples (CeO_2) are presented in Fig. 5. The H_2-TPR results demonstrate that Co doped improved the oxygen buffering capability, which considered the key for the superior DOSC performance. According to literature [6,13], the reduction of Co_3O_4 is described as a two steps process $Co_3O_4 \rightarrow CoO \rightarrow Co$. For CeO_2, the H_2 consumption peaks are observed at 511 and 801 K, respectively, which are attributed to the reduction of the surface oxygen and the bulk oxygen. It is known that CoO_x can be reduced easily in the presence of CeO_2 [13]. Synergistic interaction between Ce and Co in the mixed solid solution gives rise to low temperature reduction. The H_2-TPR analysis reveals that the reduction peaks shift to lower temperatures when Co is doped. As illustrated in Fig. 5, four reduction peaks at 276 (α), 337 (β), 501 (γ) and 791 °C (δ) can be observed for $Co_{0.05}Ce_{0.95}O_y$ sample, and the four peaks are at 277, 329, 423 and 802 °C for $Co_{0.1}Ce_{0.9}O_y$ sample. The α and β peaks can be ascribed to the step-wise reduction of cobalt oxide [6,13]. When Co is incorporated into the CeO_2 lattice to substitute Ce^{4+} cations, a solid solution is formed. The charge unbalance and lattice distortion take place within the structure of CeO_2, and thus lead to the generation of oxygen vacancies, which can bond less stable oxygen species. These weaker (active) adsorbates are reduced by H_2 at lower temperatures. The γ peak can be attributed to the

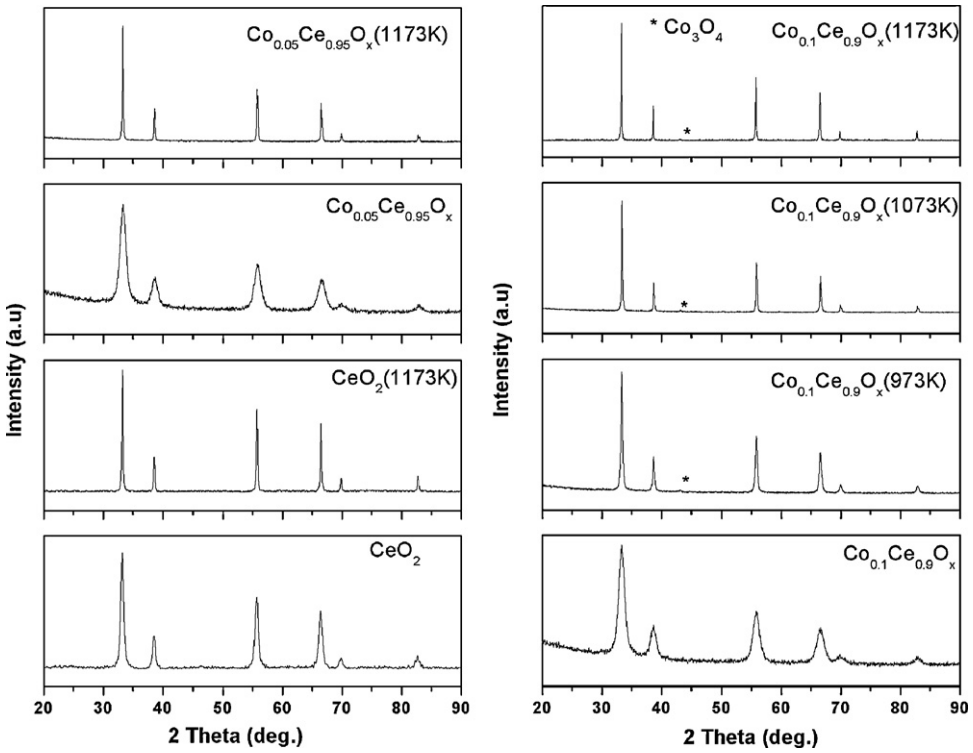

Fig. 4. XRD pattern of different samples.

Table 2
The amount of oxygen releasing in different temperature range by H_2-TPR.

Samples	The content of oxygen releasing (mmol/g)			
	<400 °C	400–600 °C	>600 °C	TOSC
$Co_{0.05}Ce_{0.95}O_x$	0.29	0.20	0.49	0.98
$Co_{0.1}Ce_{0.9}O_x$	0.18	0.73	0.47	1.32
CeO_2	0	0.27	0.61	0.88

reduction of surface/subsurface oxygen species of ceria. It suggests that there is a certain synergistic interaction between Co–O and Ce–O. The oxygen species being able to be reduced in such a range of temperatures are believed to make major contributions to DOSC and DOSR performances. The mutual promotion effect of ceria and Co species is believed to be essential for the higher DOSC and DOCR of the Co-doped samples. The δ peak represents the release of the bulk oxygen of ceria.

To derive the effect of substituting transition metal ions in ceria lattice on its oxygen storage/release property, the total oxygen storage capacity (TOSC) was estimated by the integrated amount of H_2 consumed during the H_2-TPR test. The results are listed in Table 2 along with ceria consumed 0.88 mmol/g. TOSC is related to the contents and the reducibility of the ceria components in certain materials. Although the ceria content is lowered in the Co doped samples, the TOSC was improved due to the contribution of Co dopants and its synergistic effect with Ce. It noteworthy that the amount of oxygen released at low temperatures for samples by cobalt doping was much higher than that of CeO_2, indicating the favored oxygen releasing kinetics at low temperature for Co doped samples.

3.2. Dynamic oxygen storage capacity

3.2.1. Total OSC with CO–He pulses

To study the total amount of lattice oxygen available under anaerobic atmosphere, CO pulses with He intervals were used to monitor the oxygen migration behavior of the catalysts. Fig. 6 depicts the OSC data in transient CO–He pulses. The amount of produced OSC decreases with increasing number of pulses. TOSC is calculated by adding up the OSCs during the ten consecutive CO pulses. The TOSC are increased with increasing dopant amount. In line with the previous observation, the values of specific surface areas have limited correlation with the OSC activities [19].

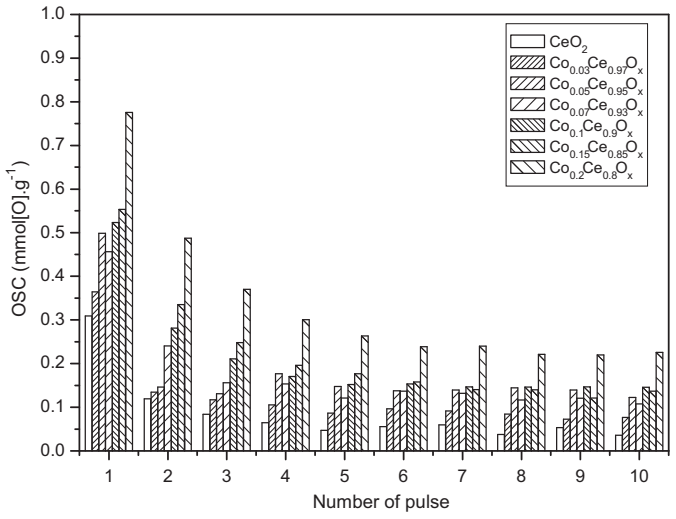

Fig. 6. OSC performance of different samples with alternate pulses of 4% CO/1% Ar/He and pure He at 500 °C.

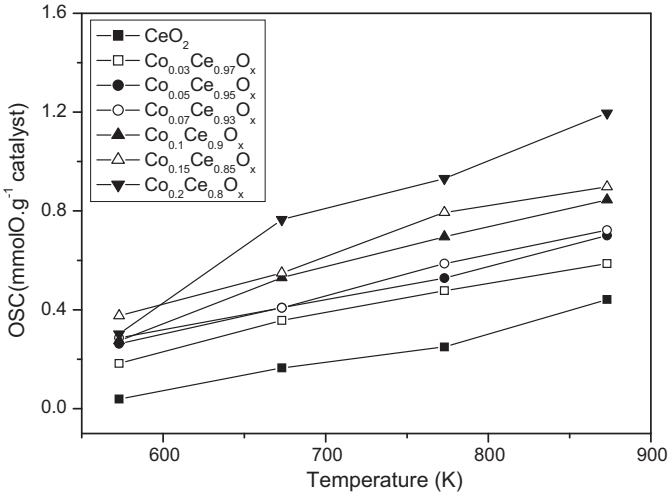

Fig. 7. Effect of Co doping on the DOSC with alternate dynamic pulses of 4% CO/1% Ar/He and 2% O_2/1% Ar/He under 0.1 Hz.

During initial CO pulses, CO oxidation occurs mostly by using the surface and near-surface oxygen of the catalysts. After the depletion of such a kind of oxygen species, the rest of the CO pulses are mostly oxidized by bulk oxygen in a two-step process, including the adsorption of CO on the catalyst' surface and its subsequent combination with bulk oxygen species. Bulk oxygen migration is the rate-determining step here, which can be considered as a function of the intrinsic structure of the material [20]. A direct relationship between lattice defects and OSC was discussed by Mamontov et al. [21] and they suggest that oxygen defects are the sources of OSC in ceria-based material. Moreover, microstructure variation of ceria-based materials induced by doping with aliovalent oxides could improve lattice oxygen mobility [22]. This is the primary reason that ceria-based oxide doping by aliovalent ions are being used in TWC as the improved generations of promoters or support oxides.

In the CeO_2 fluorite structure, cations are in 8-fold coordination with their nearest neighbors and each anion is surrounded tetrahedrally by four cations. The $Co_xCe_{1-x}O_y$ solid solution of the fluorite-type oxides is obtained by the substitution of Co cations for Ce cations. Doping the fluorite oxide with aliovalent cations, whose valency is smaller than that of the host cation, creates oxygen vacancies to achieve electronically neutrality in the substituted fluorite lattice. The presence of oxygen vacancy is the key factor for bulk oxygen mobility. According to Gupta et al. [2], the dopant Co ion in CeO_2 leads to formation of longer Co–O and Ce–O bonds. The structural distortion induced by dopant ions substitution result in enhanced DOSC performance compared to pure ceria. However, redundant Co doping would influence the catalytic activity.

3.2.2. Dynamic OSC with CO and O_2 pulses

The DOSC measurement can simulate the real operating conditions that the exhaust gas composition rapidly oscillates between reducing and oxidizing environment. So, oxidation of CO carried out under oscillating conditions is done on all the samples and the results are shown in Fig. 7. It is obvious that the DOSC of Co doped samples are higher than those of corresponding CeO_2. It suggests that the oxygen vacancies and the lattice distortion are produced by Co doped for charge compensation and radius effect, which is the essential reason for OSC promotion [1]. Further, transition metal oxide can store/release oxygen under redox conditions, which are contributed to the superior OSC performance. So we can concluded that Co doped may promote formation of Ce^{3+} ions due to the smaller size of cobalt cations that take part in removing the

Table 3
DOSR for $Co_xCe_{1-x}O_y$ samples.

Catalysts	DOSR(μmol $O g_{cat}^{-1} s$)			
	300 °C	400 °C	500 °C	600 °C
$Co_{0.05}Ce_{0.95}O_x$	9.5	17.7	24.4	36.0
$Co_{0.1}Ce_{0.9}O_x$	9.5	9.6	14.8	26.2
$Co_{0.15}Ce_{0.85}O_x$	14.6	23.7	33.4	42.3
$Co_{0.2}Ce_{0.8}O_x$	19.0	22.6	29.6	45.2
CeO_2	0	8.8	12.0	27.4

strain associated with the increase of ionic size accompanying the $Ce^{4+} \rightarrow Ce^{3+}$ transition.

Generally, DOSC can be enhanced with increasing reaction temperatures, because higher amount of lattice oxygen becomes available for the reactions and the oxygen spillover processes have been accelerated [23]. At low temperatures (below 300 °C), the surface and near-surface oxygen makes major contribution to DOSC activity. At higher temperatures (above 300 °C), bulk oxygen migration plays an important role to determine the DOSC performance. The bulk oxygen migration capability is promoted by the introduction of Co, as indicated by the improved DOSC performances of $Co_xCe_{1-x}O_y$ samples especially at high temperatures. It is noted that the DOSC does not linearly increase with the dopant amount. This would mean that the increasing presence of Co at the surface modifies the interaction with oxygen. Probably, this is related to the intrinsic arrangement of the dopant–vacancy pair, which would make bulk diffusion more difficult with respect to optimum Co doping samples.

3.2.3. Dynamic oxygen storage rate (DOSR)

As suggested by Hori et al. [24] and Fan et al. [25], the dynamic oxygen storage rate defined as the amount of oxygen stored and released in the first second of every oscillation cycle and acted as a method to characterize oxygen storage material performance. DOSR can be calculated as:

$$\text{DOSR} = \int_0^1 CO_2 \quad \text{signal} = \text{Rate} \quad [\mu\text{mol} \quad CO_2\, s^{-1}]$$

where $\int_0^1 CO_2$ signal is the integrated CO_2 peak area from 0 to 1 s.

The results of DOSR over all samples are summarized in Table 3. It is obvious that the DOSR of samples containing Co are superior to those of corresponding CeO_2. The presence of Co ions near Ce^{4+} site coordinated with O^{2-} make the transformation of $Ce^{4+} \rightarrow Ce^{3+}$ easier than ceria, since low valance cobalt cations will disturb the charge equilibrium and distortion in ceria lattice resulting in the oxygen vacancies formation associated with Ce^{3+} sites [26]. Energy between Ce^{4+} and Ce^{3+} couple is inferred to be altered by Co disturbing. Role of oxygen vacancies and lattice distortion for DOSC promotion should not be excluded by Co introducing. It should be noted that the DOSR are not linearly increased with the dopants content, in agreement with the DOSC results. It suggested that the surface Co-enrichment is formed, when the cobalt dopants content are in excess of solubility limits, which can baffle the oxygen mobility.

3.2.4. Kinetics analysis

To better understand the effect of Co doping for specific reaction procedures, kinetic parameters were investigated. Fig. 8 shows the relationship between the $\ln k$ and $1/T$ (10^3). As the reaction rate constant of CO oxidation, k is calculated by dividing from DOSR. Fitting reaction rate data to the Arrhenius equation provides the pre-exponential factors ($\ln A$) and activation energies (E_a). As listed in Table 4, the order of E_a for different samples is inconsistent with the order of the overall CO oxidation activities. This contradiction

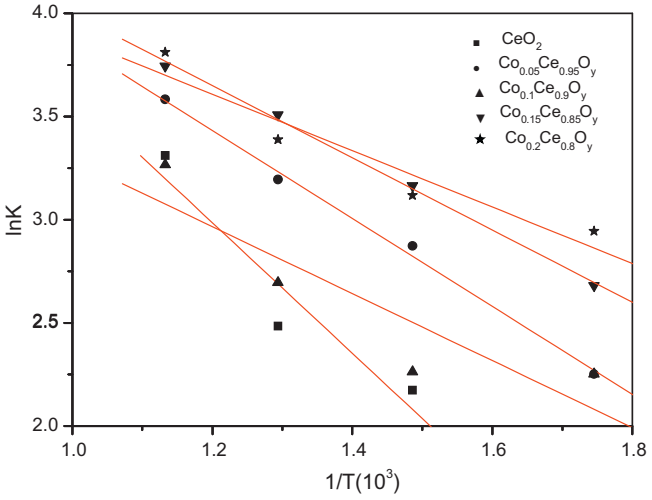

Fig. 8. Arrhenius plot of $Co_xCe_{1-x}O_y$ samples.

Table 4
The pre-exponential factor and apparent activation energy calculated for $Co_xCe_{1-x}O_y$ samples.

Catalysts	E_a (kJ mol^{-1})	$\ln A$
$Co_{0.05}Ce_{0.95}O_x$	17.7 ± 0.8	6.0 ± 0.1
$Co_{0.1}Ce_{0.9}O_x$	13.5 ± 4.8	4.9 ± 0.8
$Co_{0.15}Ce_{0.85}O_x$	14.5 ± 0.5	5.7 ± 0.1
$Co_{0.2}Ce_{0.8}O_x$	11.4 ± 2.5	5.2 ± 0.4
CeO_2	26.8 ± 8.3	6.8 ± 1.3

is induced by the compensation effect [27–29]. The linear correlations between E_a and $\ln k$ for different samples are illustrated in Fig. 9. According to the compensation effect, if the relations of the specific activation energies and the pre-exponential factors of a specific reactant for all the types of the catalysts can be fitted into a straight line, the specific reactant will be converted through the similar reaction pathways, replying on the same kind of active centers over different types of catalysts. This means that an increase of the frequency factor (consequent increase of the reaction rate) can be compensated with an increase of the activation energy. Therefore, the order of the overall reaction performances may not always be correlated positively with the absolute values of the apparent

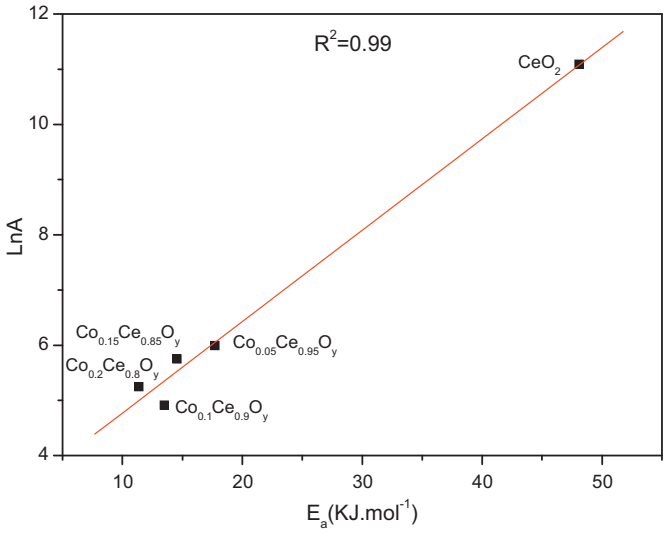

Fig. 9. Compensation effect for CO oxidation of different catalysts.

activation energies. Such an effect is mainly contributed by the heterogeneity of the surface with multiple active sites. The availability of these active sites not only changes with temperature, but also undergoes further modifications induced by the evolutions of reactants and products in gas phases [30]. As can be seen in Fig. 9, all the points can be fitted in a linear way with limited errors, suggesting the reactions over different types of catalysts investigated in this work share the similar chemical mechanisms. In this work, because the strength of adsorption is weak or the surface coverage by adsorbates is low, the changes of E_a may be mainly caused by different adsorption enthalpies, which cannot reflect the overall catalytic activity [29,30].

4. Conclusion

$Co_xCe_{1-x}O_y$ with different Co/Ce atomic ratio (1–20 mol%) were prepared by sol–gel method. The powder XRD data following Rietveld refinement revealed that the solubility limit of cobalt oxides in the CeO_2 was 5 mol%. The thermal stability results revealed that the redundant cobalt species separated out of the CeO_2 and interacted with the ceria species on the surface, which seriously influenced the oxygen handling properties. DOSC results revealed Ce-based materials containing cobalt oxides with multiple valences contribute to the majority of DOSC. From kinetic analysis, the confirmation of compensation effect revealed that all catalysts share the same mechanism for the separated reactions we investigated.

Acknowledgement

The authors are grateful to the support the National High-Tech Research and Development Program of China (2009AA064803) and the Program of Introducing Talents of Discipline to Universities (no. B06006).

References

[1] A. Trovarelli, Catal. Rev. Sci. Eng. 38 (1996) 439.
[2] A. Gupta, U.V. Waghmare, M.S. Hegde, Chem. Mater. 22 (2010) 5184.
[3] J.J. Spivey, Ind. Eng. Chem. Res. 26 (1987) 2165.
[4] M.M. Natile, A. Glisenti, J. Mol. Catal. A: Chem. 217 (2004) 175.
[5] C.N. Satterfeld, Heterogeneous Catalysis in Industrial Practice, 2nd ed., McGraw-Hill, New York, 1991 (Chapter 8).
[6] M. Kang, M.W. Song, C.H. Lee, Appl. Catal. A 251 (2003) 143.
[7] X.Y. Xu, J.J. Li, Z.P. Hao, J. Rare Earth 2 (2006) 172.
[8] M.M. Natile, A. Glisenti, Chem. Mater. 17 (2005) 3403.
[9] L.F. Liotta, G. Di Carlo, G. Pantaleo, A.M. Venezia, G. Deganello, Appl. Catal. B 66 (2006) 217.
[10] B.H. Yue, R.X. Zhou, Y.J. Wang, X.M. Zheng, Appl. Surf. Sci. 252 (2006) 5820.
[11] L.F. Liotta, G. Di Carlo, G. Pantaleo, G. Deganello, Appl. Catal. B 70 (2007) 314.
[12] L. Xue, C.B. Zhang, H. He, Y. Teraoka, Appl. Catal. B 75 (2007) 167.
[13] L. Spadaro, F. Arena, M.L. Granados, J. Catal. 234 (2005) 451.
[14] G.F. Li, Q.Y. Wang, B. Zhao, R.X. Zhou, J. Mol. Catal. A: Chem. 326 (2010) 69.
[15] F.B. Noronha, M.C. Durão, M.S. Batista, Catal. Today 85 (2003) 13.
[16] Z.Q. Han, J.Q. Wang, H.J. Yan, M.Q. Shen, J. Wang, W.L. Wang, M. Yang, Catal. Today 158 (2010) 481.
[17] D.J. Kim, J. Am. Ceram. Soc. 72 (1989) 1415.
[18] V.B. Glushkova, F. Hanic, L.V. Sazonova, Ceramurgia Int. 4 (1978) 176.
[19] E. Aneggi, J. Llorca, M. Boaro, J. Catal. 234 (2005) 88.
[20] H. Vidal, J. Kašpar, M. Pijolat, Appl. Catal. B 30 (2001) 75.
[21] E. Mamontov, T. Egami, R. Brezny, J. Phys. Chem. B 104 (2000) 11110.
[22] P. Fornasiero, E. Fonda, R. Di Monte, J. Catal. 187 (1999) 177.
[23] M.W. Zhao, M.Q. Shen, J. Wang, J. Catal. 248 (2007) 258.
[24] C.E. Hori, A. Brenner, K.Y. Simon Ng, K.M. Rahmoeller, D. Belton, Catal. Today 50 (1999) 299.
[25] J. Fan, D. Weng, X.D. Wu, X.D. Wu, R. Ran, J. Catal. 258 (2008) 177.
[26] M. Fernández-García, A. Martínez-Arias, A. Guerrero-Ruiz, C. Conesa, J. Soria, J. Catal. 211 (2002) 326.
[27] A.K. Galwey, M.E. Brown, J. Catal. 60 (1979) 335.
[28] W.R. Patterson, J.J. Rooney, J. Catal. 146 (1994) 310.
[29] G.C. Bond, M.A. Keane, H. Kral, J.A. Lercher, Catal. Rev. Sci. Eng. 42 (2000) 323.
[30] J.A. Botas, M.A. Gutiérrez-Ortiz, J.A. González-Marcos, G. Blanchard, J.R. González-Velasco, Appl. Catal. B 32 (2001) 243.